

Article

# An Accelerated Double-Integral ZNN with Resisting Linear Noise for Dynamic Sylvester Equation Solving and Its Application to the Control of the SFM Chaotic System

Luyang Han <sup>1</sup>, Yongjun He <sup>2</sup>, Bolin Liao <sup>1,\*</sup>  and Cheng Hua <sup>1</sup>

<sup>1</sup> College of Computer Science and Engineering, Jishou University, Jishou 416000, China

<sup>2</sup> School of Mathematics and Statistics, Hunan Normal University, Changsha 410081, China

\* Correspondence: bolinliao@jsu.edu.cn; Tel.: +86-137-8791-8516

**Abstract:** The dynamic Sylvester equation (DSE) is frequently encountered in engineering and mathematics fields. The original zeroing neural network (OZNN) can work well to handle DSE under a noise-free environment, but may not work in noise. Though an integral-enhanced zeroing neural network (IEZNN) can be employed to solve the DSE under multiple-noise, it may fall flat under linear noise, and its convergence speed is unsatisfactory. Therefore, an accelerated double-integral zeroing neural network (ADIZNN) is proposed based on an innovative design formula to resist linear noise and accelerate convergence. Besides, theoretical proofs verify the convergence and robustness of the ADIZNN model. Moreover, simulation experiments indicate that the convergence rate and anti-noise ability of the ADIZNN are far superior to the OZNN and IEZNN under linear noise. Finally, chaos control of the sine function memristor (SFM) chaotic system is provided to suggest that the controller based on the ADIZNN has a smaller amount of error and higher accuracy than other ZNNs.

**Keywords:** dynamic Sylvester equation; linear noise; accelerated double integral ZNN; chaos control

**MSC:** 15A24; 34A34; 34H10; 93D20



**Citation:** Han, L.; He, Y.; Liao, B.; Hua, C. An Accelerated Double-Integral ZNN with Resisting Linear Noise for Dynamic Sylvester Equation Solving and Its Application to the Control of the SFM Chaotic System. *Axioms* **2023**, *12*, 287. <https://doi.org/10.3390/axioms12030287>

Academic Editors: Nuno Bastos, Touria Karite and Amir Khan

Received: 3 February 2023

Revised: 23 February 2023

Accepted: 3 March 2023

Published: 9 March 2023



**Copyright:** © 2023 by the authors. Licensee MDPI, Basel, Switzerland. This article is an open access article distributed under the terms and conditions of the Creative Commons Attribution (CC BY) license (<https://creativecommons.org/licenses/by/4.0/>).

## 1. Introduction

The Sylvester equation is a crucial matrix equation. It has a crucial position in many fields, such as image fusion [1], object detection [2], control configuration selection [3], fast tensor product solution [4], robotics [5–8], permanent magnet synchronous motors [9] and mobile manipulators [10]. Therefore, finding a quick solution to handle the dynamic Sylvester equation (DSE) is exceptionally crucial. Many scholars previously utilized numerical methods to solve the Sylvester equation, such as the Hessenberg–Schur iteration method [11] and Krylov subspace methods [12]. Nevertheless, numerical methods are only suitable for small-scale matrix issues and cannot solve DSE well. In recent years, the advantages of feedforward neural networks and recurrent neural networks (RNNs) with the parallel process and easy implementation in hardware have been gradually excavated [13–16]. The gradient neural network (GNN), an important type of RNN, has become increasingly popular in high-dimensional Sylvester equation solving [17,18]. Nevertheless, when the GNN approach was extended to dynamic domains, researchers discovered the two defects of GNN: first, the GNN method cannot make the residual value reach zero; second, its convergence rate is deficient.

After that, the original zeroing neural network (OZNN) was reported, aiming at the shortcomings of the GNN [19]. With the development of the zeroing neural network (ZNN) model, many scholars have focused on ZNN because it can deal with many dynamic mathematical problems [20–22]. Simultaneously, scholars constantly improved and innovated on the basis of the ZNN and they obtained many derived ZNN models for specific problems [7,9,23–25]. For instance, He et al. presented a double-accelerated ZNN for

handling dynamic matrix inversion [23]. Xiao et al. proposed two nonlinear ZNN models and applied them to the 3D moving target location [24]. A noise-suppression variable parameter ZNN was proposed to handle the DSE [26]. In addition, there is much related work on the universal DSE [27,28].

It is worth noting that noise cannot be ignored, and it will affect the stability of the system [29–31]. Therefore, we should consider both convergence and robustness when designing ZNN models [32–34]. In order to better suppress noise, the PID control method is usually used by the public [35]. The control principle also mentions that the integral term can eliminate noise so that the error in the system is continuously reduced. Thus, the integral-enhanced ZNN model (IEZNN) was designed [32], and the integral term made up for the defect that the original ZNN could not suppress noise. Besides, many anti-noise ZNNs were researched and applied [36–38].

Nevertheless, the IEZNN model cannot suppress linear noise well. Many researchers point out that the activation functions can accelerate convergence and suppress noise [39–41]. Utilizing double integration and the fixed-time activation function (FTAF), we propose an accelerated double integral ZNN (ADIZNN) model with anti-linear noise interference to settle the DSE under linear noise. In brief, the ADIZNN has the characteristic of accelerated convergence and enhanced robustness due to the introduction of the FTAF and the double integral term. In addition, the theoretical proofs and simulation experiments under the linear noise environments are given. At last, the design ideas of ZNNs are extended to chaos control of the SFM chaotic system to show that the controller based on the ADIZNN has significant advantages compared with other controllers.

The remaining part of this paper is divided into five sections. Section 2 introduces the OZNN, IEZNN and ADIZNN models. Theoretical analyses of the ADIZNN are provided in Section 3. Section 4 offers two specific examples under linear noise. Besides, the chaos control experiment of the SFM chaotic system is provided in Section 5. Section 6 is the summary part of paper. These are the significant contributions of this research.

- Based on the novel ZNN design formula, an innovative ADIZNN is constructed for settling the dynamic Sylvester equation under the linear noise.
- The ADIZNN model has a novel double integral structure and activation function, which guarantees accelerated convergence and enhanced anti-noise capacity.
- Theoretical analyses and simulation results are provided to ensure that the ADIZNN model can handle the DSE with excellent convergence and robustness.
- Chaos control schemes of the TFM chaotic system are established to display that the controller based on the ADIZNN has superior performance than that based on the OZNN and IEZNN.

## 2. DSE Description and Models Design

Firstly, the general dynamic Sylvester equation (DSE), OZNN and IEZNN are offered. Posteriorly, the novel ADIZNN model proposed is particularly elaborated.

### 2.1. Description of DSE

The definition of the DSE is described in detail as follows:

$$U(t)P(t) - P(t)V(t) + G(t) = 0, \quad (1)$$

in which  $U(t), V(t), G(t) \in \mathbb{R}^{n \times n}$  are time-varying matrices, and  $P(t) \in \mathbb{R}^{n \times n}$  is an unknown matrix.

The purpose of the ZNN model is to solve the unknown  $P(t)$  in Equation (1) under noise, and the theoretical solution is denoted by  $P^*(t)$ . Moving matrix  $G(t)$  of (1), we have

$$U(t)P(t) - P(t)V(t) = -G(t). \quad (2)$$

For further derivation, we need to vectorize Equation (2) and obtain

$$(I_n \otimes U(t) - V^T(t) \otimes I_n) \text{vec}(P(t)) = -\text{vec}(G(t)), \tag{3}$$

in which  $I_n \in \mathbb{R}^{n \times n}$  is an identity matrix, and  $\text{vec}(\cdot)$  and the symbol  $\otimes$  signify the vectorization and Kronecker product operation. Setting  $Q(t) = I_n \otimes U(t) - V^T(t) \otimes I_n \in \mathbb{R}^{nm \times nm}$ ,  $p(t) = \text{vec}(P(t)) \in \mathbb{R}^{nm \times 1}$ ,  $g(t) = \text{vec}(G(t)) \in \mathbb{R}^{nm \times 1}$  of (3), the DSE is transformed into a linear equation:

$$Q(t)p(t) = -g(t).$$

For monitoring the solution process, we define

$$W(t) = Q(t)p(t) + g(t) \tag{4}$$

as an error function. The derivative of (4) with respect to time can be written as

$$\dot{W}(t) = \dot{Q}(t)p(t) + Q(t)\dot{p}(t) + \dot{g}(t). \tag{5}$$

### 2.2. Relevant Models Design

A detailed description of the relevant models are introduced in this subsection. The design formula of error in the ZNN model is defined as

$$\dot{W}(t) = -\zeta \Phi(W(t)), \tag{6}$$

in which  $\zeta \in \mathbb{R}^+$  and  $\Phi(\cdot)$  is a mapping array composed by the activation function. The elemental form of (6) is as follows

$$\dot{w}_i(t) = -\zeta \phi(w_i(t)),$$

where  $\phi(\cdot)$  denotes the nonlinear monotone non-decreasing odd activation function, and  $w_i(\cdot)$  and  $\phi(\cdot)$  are element forms of the  $W(\cdot)$  and  $\Phi(\cdot)$ , where  $i = 1, 2, \dots, n^2$ . When  $\phi(\cdot)$  is the linear activation function (i.e.,  $\phi(t) = t$ ), we get the design formula of the OZNN model:

$$\dot{W}(t) = -\zeta W(t). \tag{7}$$

Considering the case of linear noise, the design formula of the OZNN is

$$\dot{W}(t) = -\zeta W(t) + Z(t), \tag{8}$$

where  $Z(t) \in \mathbb{R}^{nm \times 1}$  refers to linear noise. Linear noise is a significant kind of noise, and it is generally shaped like  $Z(t) = At + B$ , where  $A, B \in \mathbb{R}^{nm \times 1}$ . Let  $z_i(t)$ ,  $a_i$  and  $b_i$  stand for the  $i$ th elements of  $Z(t)$ ,  $A$  and  $B$ . Then, the element form of  $Z(t)$  is rewritten as  $z_i(t) = a_i t + b_i$ . Substituting Equations (4) and (5) into (8), the OZNN model to solve the DSE is obtained

$$Q(t)\dot{p}(t) = -\dot{Q}(t)p(t) - \dot{g}(t) - \zeta(Q(t)p(t) + g(t)) + Z(t). \tag{9}$$

On this basis, Jin et al. added an integral term to suppress the noise and proposed an integral-enhanced ZNN (IEZNN) [32], and its design formula is

$$\dot{W}(t) = -\zeta W(t) - \lambda \int_0^t W(\tau) d\tau, \tag{10}$$

with  $\zeta$  and  $\lambda \in \mathbb{R} > 0$ . Then, we obtain the case of (10) under noise:

$$\dot{W}(t) = -\zeta W(t) - \lambda \int_0^t W(\tau) d\tau + Z(t). \tag{11}$$

Substituting (4) and (5) into (11), the model of the IEZNN can be rewritten as

$$Q(t)\dot{p}(t) = -\dot{Q}(t)p(t) - \dot{g}(t) - \zeta(Q(t)p(t) + g(t)) - \lambda \int_0^t (Q(\tau)p(\tau) + g(\tau))d\tau + Z(t). \tag{12}$$

Now that all the relevant models descriptions are complete, the accelerated double integral ZNN will be introduced.

### 2.3. ADIZNN Model Design

In this subsection, an accelerated double integral ZNN (ADIZNN) model is proposed, which can resist the linear noise effectively. We know that  $\dot{W}(t) = -\zeta\Phi(W(t))$  from Section 2.2, to describe the evolution of the model more intuitively, set

$$\Theta(t) = \dot{W}(t) + \zeta\Phi(W(t)), \tag{13}$$

where  $\Phi(\cdot)$  denotes the fixed-time activation function (FTAF) here, and its element form is

$$\phi(i) = (\varepsilon_1|i|^\mu + \varepsilon_2|i|^\sigma)\text{sign}(i) + \varepsilon_3i + \varepsilon_4\text{sign}(i), \tag{14}$$

in which  $\varepsilon_1$  and  $\varepsilon_2 > 0$ ,  $\varepsilon_3$  and  $\varepsilon_4 \geq 0$ ,  $0 < \mu < 1, \sigma > 1$ .

**Remark 1.** We make some detailed remarks about FTAF (14).

- The  $\varepsilon_1|i|^\mu\text{sign}(i)$  and  $\varepsilon_2|i|^\sigma\text{sign}(i)$  of FTAF (14) are to accelerate convergence.
- The  $\varepsilon_3i$  and  $\varepsilon_4\text{sign}(i)$  of FTAF (14) are to suppress noise;

In addition, let

$$\Theta(t) = -\lambda \int_0^t \Theta(\tau)d\tau,$$

with  $\lambda \in \mathbb{R}^+$ . We define

$$Y(t) = \Theta(t) + \lambda \int_0^t \Theta(\tau)d\tau. \tag{15}$$

Substituting (13) into (15), one can get

$$Y(t) = \dot{W}(t) + \zeta\Phi(W(t)) + \lambda \int_0^t (\dot{W}(\tau) + \zeta\Phi(W(\tau)))d\tau. \tag{16}$$

Similarly, set

$$Y(t) = -\lambda \int_0^t Y(\tau)d\tau. \tag{17}$$

Substituting (16) into (17), we obtain

$$\begin{aligned} & \dot{W}(t) + \zeta\Phi(W(t)) + \lambda W(t) + \lambda\zeta \int_0^t \Phi(W(\tau))d\tau \\ &= -\lambda \int_0^t \left( \dot{W}(\tau) + \zeta\Phi(W(\tau)) + \lambda W(\tau) + \lambda\zeta \int_0^\tau \Phi(W(\sigma))d\sigma \right) d\tau \\ &= -\lambda W(t) - \lambda\zeta \int_0^t \Phi(W(\tau))d\tau - \lambda^2 \int_0^t W(\tau)d\tau - \lambda^2\zeta \int_0^t \int_0^\tau \Phi(W(\sigma))d\sigma d\tau. \end{aligned}$$

Thus, the design formula of the ADIZNN for DSE is obtained:

$$\begin{aligned} \dot{W}(t) = & -2\lambda W(t) - \zeta\Phi(W(t)) - \lambda^2 \int_0^t W(\tau)d\tau \\ & - 2\lambda\zeta \int_0^t \Phi(W(\tau))d\tau - \lambda^2\zeta \int_0^t \int_0^\tau \Phi(W(\sigma))d\sigma d\tau. \end{aligned} \tag{18}$$

Furthermore, the design formula of the ADIZNN with noise can be written as

$$\begin{aligned} \dot{W}(t) = & -2\lambda W(t) - \xi\Phi(W(t)) - \lambda^2 \int_0^t W(\tau)d\tau \\ & - 2\lambda\xi \int_0^t \Phi(W(\tau))d\tau - \lambda^2\xi \int_0^t \int_0^\tau \Phi(W(\sigma))d\sigma d\tau + Z(t). \end{aligned}$$

Furthermore,  $W(t) = Q(t)p(t) + g(t)$  and  $\dot{W}(t) = \dot{Q}(t)p(t) + Q(t)\dot{p}(t) + \dot{g}(t)$  are already known. Hence, the ADIZNN model that included noise can be further obtained:

$$\begin{aligned} Q(t)\dot{p}(t) = & -\dot{Q}(t)p(t) - \dot{g}(t) - 2\lambda(Q(t)p(t) + g(t)) - \xi\Phi(Q(t)p(t) + g(t)) \\ & - 2\lambda\xi \int_0^t \Phi(Q(\tau)p(\tau) + g(\tau))d\tau - \lambda^2 \int_0^t (Q(\tau)p(\tau) + g(\tau))d\tau \quad (19) \\ & - \lambda^2\xi \int_0^t \int_0^\tau \Phi(\dot{Q}(\sigma)p(\sigma) + Q(\sigma)\dot{p}(\sigma) + \dot{g}(\sigma))d\sigma d\tau + Z(t). \end{aligned}$$

**Remark 2.** We make some detailed remarks about ADIZNN (19).

- Based on the novel ZNN design formula, an innovative ADIZNN is constructed for settling the DSE under the linear noise.
- The novel double integral structure and activation function, which guarantees accelerated convergence and enhanced anti-noise capacity.

### 3. Theoretical Analyses

We mainly discuss and prove properties of the ADIZNN in this section. In order to better express the Frobenius norm of  $W(t)$ , we introduce the error norm  $\|W(t)\|_F = \|Q(t)p(t) + g(t)\|_F$ .

#### 3.1. Convergence

The convergence performance of ADIZNN (19) is investigated and studied under the ideal noise-free condition in this subsection.

**Theorem 1.** Given matrices  $U(t) \in \mathbb{R}^{n \times n}$ ,  $V(t) \in \mathbb{R}^{n \times n}$  and  $G(t) \in \mathbb{R}^{n \times n}$ . From any initial value  $P(0)$ , the error norm  $\|W(t)\|_F$  of ADIZNN (19) can reach zero under the ideal noise-free condition, that is,

$$\lim_{t \rightarrow \infty} \|W(t)\|_F = 0.$$

**Proof of Theorem 1.** In order to give a clearer proof process, let  $w_i(t)$ ,  $\theta_i(t)$ ,  $\gamma_i(t)$  and  $\phi(\cdot)$  represent the elements form of  $W(t)$ ,  $\Theta(t)$ ,  $Y(t)$  and  $\Phi(\cdot)$ . First, considering

$$Y(t) = \dot{W}(t) + \xi\Phi(W(t)) + \lambda \int_0^t (\dot{W}(\tau) + \xi\Phi(W(\tau)))d\tau, \quad (20)$$

ADIZNN model (19) under the noiseless environment can be transformed into

$$Y(t) = -\lambda \int_0^t Y(\tau)d\tau. \quad (21)$$

The element form of (21) is

$$\gamma_i(t) = -\lambda \int_0^t \gamma_i(\tau)d\tau. \quad (22)$$

Then, the derivative of (22) is

$$\dot{\gamma}_i(t) = -\lambda\gamma_i(t). \quad (23)$$

Setting a Lyapunov equation

$$\ell(t) = \gamma_i^2(t),$$

its derivative is

$$\dot{\ell}(t) = 2\dot{\gamma}_i(t)\gamma_i(t). \tag{24}$$

Substituting (23) into (24), we have

$$\dot{\ell}(t) = -2\lambda\gamma_i(t)\gamma_i(t) = -2\lambda\gamma_i^2(t).$$

Because  $\ell(t)$  is positive definite and  $\dot{\ell}(t)$  is negative definite,  $\ell(t)$  is globally asymptotically stable, and we have

$$\lim_{t \rightarrow \infty} |\ell(t)| = \lim_{t \rightarrow \infty} |\gamma_i^2(t)| = \lim_{t \rightarrow \infty} |\gamma_i(t)| = 0. \tag{25}$$

Thus,  $\gamma_i = \dot{w}_i(t) + \xi\phi(w_i(t)) + \lambda \int_0^t (\dot{w}_i(\tau) + \xi\phi(w_i(\tau)))d\tau = 0$  as  $t \rightarrow \infty$  based on (20) and (25). Considering  $\theta_i(t) = \dot{w}_i(t) + \xi\phi(w_i(t))$ , then we have

$$\theta_i(t) = -\lambda \int_0^t \theta_i(\tau)d\tau, t \rightarrow \infty. \tag{26}$$

Therefore,

$$\lim_{t \rightarrow \infty} \left| \theta_i(t) + \lambda \int_0^t \theta_i(\tau)d\tau \right| = 0.$$

It is not difficult to know

$$\lim_{t \rightarrow \infty} |\theta_i(t)| = \lim_{t \rightarrow \infty} \left| -\lambda \int_0^t \theta_i(\tau)d\tau \right|.$$

The derivative of the above equation is

$$\lim_{t \rightarrow \infty} |\dot{\theta}_i(t)| = \lim_{t \rightarrow \infty} |-\lambda\theta_i(t)| + \Delta, \Delta \rightarrow 0,$$

where  $\Delta$  is a small error in the derivative of  $\theta_i(t)$ . Setting another Lyapunov equation

$$\dot{h}(t) = \theta_i^2(t). \tag{27}$$

The derivative of (27) is

$$\dot{h}(t) = 2\dot{\theta}_i(t)\theta_i(t) = -2\lambda\theta_i^2(t).$$

According to the Lyapunov theorem, we get

$$\lim_{t \rightarrow \infty} |\theta_i(t)| = 0.$$

Because  $\theta_i(t) = \dot{w}_i(t) + \xi\phi(w_i(t))$ , thus,

$$\lim_{t \rightarrow \infty} |\theta_i(t)| = \lim_{t \rightarrow \infty} |\dot{w}_i(t) + \xi\phi(w_i(t))| = 0. \tag{28}$$

Thus,

$$\dot{w}_i(t) = -\xi\phi(w_i(t)).$$

Clearly, we get

$$\lim_{t \rightarrow \infty} |w_i(t)| = 0.$$

Thus, writing it in matrix form gives the following

$$\lim_{t \rightarrow \infty} \|W(t)\|_F = 0.$$

The proof is completed now.  $\square$

### 3.2. Robustness

Furthermore, the ADIZNN model can still approximate the theoretical solution infinitely when solving the DSE in a noisy environment. In other words, the ADIZNN model has strong robustness. Its robustness proof process is presented below.

**Theorem 2.** *Given matrices  $U(t) \in \mathbb{R}^{n \times n}$ ,  $V(t) \in \mathbb{R}^{n \times n}$  and  $G(t) \in \mathbb{R}^{n \times n}$ , the identity matrix  $I_n \in \mathbb{R}^{n \times n}$ . From any initial value  $P(0)$ ,  $P(t)$  of the proposed ADIZNN can reach  $P^*(t)$  in solving the DSE under the linear noise condition, that is,*

$$\lim_{t \rightarrow \infty} \|W(t)\|_F = 0.$$

**Proof of Theorem 2.** Linear noise can be written as

$$Z(t) = At + B, \tag{29}$$

where  $A \in \mathbb{R}^{nn \times 1}$  and  $B \in \mathbb{R}^{nn \times 1}$  are constant matrices. Its element form can be written as

$$z_i(t) = a_i t + b_i.$$

According to (20) and (21) of Theorem 1, the ADIZNN model (19) can be converted to

$$Y(t) = -\lambda \int_0^t Y(\tau) d\tau + Z(t). \tag{30}$$

Its element is

$$\gamma_i(t) = -\lambda \int_0^t \gamma_i(\kappa) d\kappa + z_i(t). \tag{31}$$

Taking the derivative of  $\gamma_i$  twice, we get

$$\ddot{\gamma}_i(t) = -\lambda \dot{\gamma}_i(t) + \dot{z}_i(t). \tag{32}$$

Differentiating the linear noise once and twice yield  $\dot{z}_i(t) = a$  and  $\ddot{z}_i(t) = 0$ . Then,

$$\ddot{\gamma}_i(t) = -\lambda \dot{\gamma}_i(t).$$

We set up a Lyapunov function  $\mathfrak{S}(t) = \dot{\gamma}_i^2(t)$ , so

$$\dot{\mathfrak{S}}(t) = 2\dot{\gamma}_i(t)\ddot{\gamma}_i(t) = -\lambda \dot{\gamma}_i^2(t).$$

Due to the  $\mathfrak{S}(t)$  being positive definite and  $\dot{\mathfrak{S}}(t)$  being negative definite,  $\mathfrak{S}(t)$  is globally asymptotically stable, and we have

$$\lim_{t \rightarrow \infty} |\mathfrak{S}(t)| = \lim_{t \rightarrow \infty} |\dot{\gamma}_i^2(t)| = \lim_{t \rightarrow \infty} |\dot{\gamma}_i(t)| = 0. \tag{33}$$

According to (31) and (33), we obtain

$$\lim_{t \rightarrow \infty} |\dot{\gamma}_i(t)| = \lim_{t \rightarrow \infty} |-\lambda \gamma_i(t) + \dot{z}_i(t)| = 0.$$

We know that  $\dot{z}_i(t) = a$ , so it is not hard to figure out

$$\lim_{t \rightarrow \infty} |-\lambda \gamma_i(t) + a| = 0.$$

Then it is concluded that

$$\lim_{t \rightarrow \infty} |\lambda \gamma_i(t)| = |a|.$$

Thus we get

$$\lim_{t \rightarrow \infty} |\gamma_i(t)| = \left| \frac{a}{\lambda} \right|.$$

Thus  $|\gamma_i(t)| = \left| \dot{w}_i(t) + \zeta\phi(w_i(t)) + \lambda \int_0^t (\dot{w}_i(\tau) + \zeta\phi(w_i(\tau)))d\tau \right| = |a/\lambda|$  as  $t \rightarrow \infty$ . Let

$$\theta_i(t) = \dot{w}_i(t) + \zeta\phi(w_i(t)), \tag{34}$$

then we have  $|\gamma_i(t)| = \left| \theta_i(t) + \lambda \int_0^t \theta_i(\tau)d\tau \right| = |a/\lambda|$  as  $t \rightarrow \infty$ . Thus we can infer that

$$\lim_{t \rightarrow \infty} (\dot{\theta}_i(t) + \lambda\theta_i(t)) = 0.$$

Then, we can draw

$$\lim_{t \rightarrow \infty} \dot{\theta}_i(t) = \lim_{t \rightarrow \infty} -\lambda\theta_i(t).$$

Obviously, due to  $\lambda > 0$ ,  $\dot{\theta}_i(t)$  and  $\theta_i(t)$  having different signs, thus we get

$$\lim_{t \rightarrow \infty} |\theta_i(t)| = 0.$$

In addition,  $\theta_i(t) = \dot{w}_i(t) + \zeta\phi(w_i(t))$  is known from (34), that means

$$\lim_{t \rightarrow \infty} |\theta_i(t)| = \lim_{t \rightarrow \infty} |\dot{w}_i(t) + \zeta\phi(w_i(t))| = 0.$$

The above equation and (28) are the same, we can say

$$\lim_{t \rightarrow \infty} |w_i(t)| = 0.$$

The corresponding matrix form is

$$\lim_{t \rightarrow \infty} \|W(t)\|_F = 0.$$

Thus, the proof is accomplished now.  $\square$

#### 4. Examples Verification

In Section 3, the properties of the ADIZNN are proved. In this section, comparative experiments are adopted to highlight the outstanding performance of ADIZNN (19). The OZNN (9), IEZNN (12) and ADIZNN (19) models are applied in solving the dynamic Sylvester equation problem. Besides,  $P^*(t)$  refers to the theoretical value of  $P(t)$  in the experiment 1 and experiment 2.

**Remark 3.** Sylvester matrix equations play an important role in the field of control [3,42,43], and they are widely used in the fields of manipulators [10], signal processing [1,44] and statistics [45]. For example, the redundant decomposition of manipulator in the Ref. [10] can first be represented by the quadratic programming problem with equality constraints, then this problem can be further converted into a dynamic linear equation (i.e., a special case of the DSE when  $V(t) = 0$ ) by the Lagrange multiplier method. Therefore, this paper only verifies the effect of the proposed model to solve the DSE, which can be extended to related fields.

##### 4.1. Experiment 1

The dynamic matrices  $U(t)$ ,  $V(t)$  and  $G(t)$  are provided

$$U(t) = \begin{bmatrix} s(-2t) & -c(-2t) \\ c(-2t) & s(-2t) \end{bmatrix}, V(t) = \begin{bmatrix} t & 0 \\ 0 & 2 \end{bmatrix}, G(t) = \begin{bmatrix} s(3t) & c(3t) \\ 2s(3t) & -2c(3t) \end{bmatrix}, \tag{35}$$

where  $s(\cdot)$  and  $c(\cdot)$  represent the sine function and cosine function. The default model parameters are:  $\zeta = 2, \lambda = 1, \varepsilon_1 = \varepsilon_2 = \varepsilon_3 = \varepsilon_4 = 0.5$  and  $\mu = 0.5, \sigma = 2$ .

Figure 1 presents state trajectories synthesized by the OZNN model (9), IEZNN model (12) and ADIZNN model (19) using FTAF (14) for the DSE with (35) in the noiseless environment. It is obvious that the OZNN model (9), IEZNN model (12) and ADIZNN model (19) can fit the theoretical solutions in a noiseless environment. Even without linear noise, ADIZNN (19) has the fastest convergence speed, which means that its convergence performance is better than the other two models.

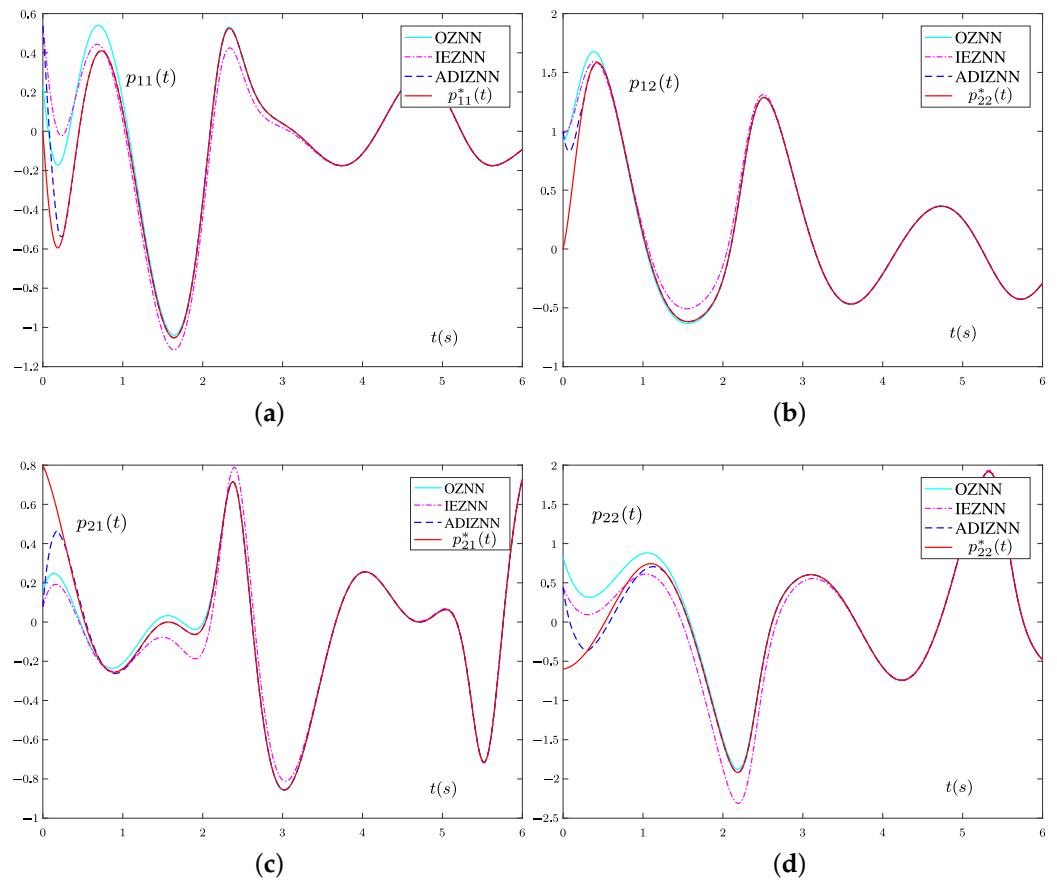


**Figure 1.** State trajectories of OZNN (9), IEZNN (12) and ADIZNN (19) for the DSE with (35) in the absence of the noise. (a) State trajectory of  $p_{11}(t)$ . (b) State trajectory of  $p_{12}(t)$ . (c) State trajectory of  $p_{21}(t)$ . (d) State trajectory of  $p_{22}(t)$ .

Although in the noiseless environment, all three models can fit the theoretical value, model testing in noisy environment is more important. In Figure 2, we explore the state trajectories of these three models under linear noise  $z_i(t) = t/4 + 4$  for the DSE with (35). Obviously, the OZNN’s state trajectory completely deviates from the theoretical results, that is to say, OZNN (9) cannot calculate the theoretical result of DSE under  $z_i(t) = t/4 + 4$ . In Figure 2, the fitting trend of IEZNN (12) is closer and closer to  $P^*(t)$  with the increase of  $t$ ,  $p_{11}(t), p_{12}(t), p_{21}(t)$  and  $p_{22}(t)$  of IEZNN (12) still cannot converge to  $p_{11}^*(t), p_{12}^*(t), p_{21}^*(t)$  and  $p_{22}^*(t)$ . However, the  $p_{11}(t), p_{12}(t), p_{21}(t)$  and  $p_{22}(t)$  of ADIZNN (19) converge to theoretical values within 1.3 s. The above results are sufficient to illustrate that ADIZNN (19) can suppress  $z_i(t) = t/4 + 4$  when solving the DSE problem.

**Remark 4.** Here, we have a discussion of the results of the comparison about Figures 1 and 2. Since the OZNN model (9) does not contain an integral term, it has no ability to suppress linear noise. The IEZNN model (12) contains an integral term, which can resist linear noise to a certain extent, and the error results obtained by solving the DSE with the IEZNN model (12) are not satisfactory.

However, the ADIZNN model (19) contains the double integral term and FTAF (14), which can effectively suppress linear noise, and its convergence time is much faster than IEZNN.

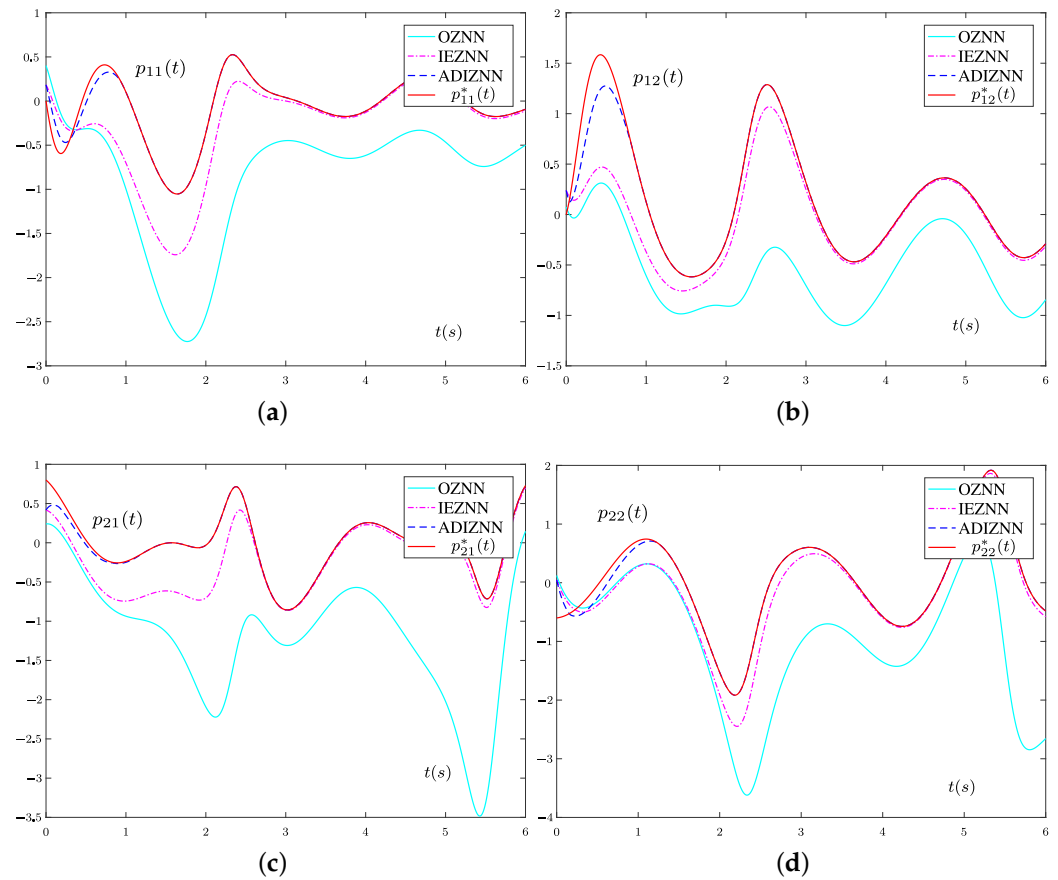


**Figure 2.** State trajectories of OZNN (9), IEZNN (12) and ADIZNN (19) for the DSE with (35) under the linear noise  $z_i(t) = t/4 + 4$ . (a) State trajectory of  $p_{11}(t)$ . (b) State trajectory of  $p_{12}(t)$ . (c) State trajectory of  $p_{21}(t)$ . (d) State trajectory of  $p_{22}(t)$ .

In Figure 3, we study the error norms  $\|W(t)\|_F$  of OZNN model (9), IEZNN model (12) and ADIZNN model (19) with  $\zeta = 2$  and  $\lambda = 1$  under the different noise environments for the two-dimensional matrices (35). Figure 3a–d correspond to  $z_i(t) = 0$ ,  $z_i(t) = t/4 + 4$ ,  $z_i(t) = 4t + 4$  and  $z_i(t) = 16t + 4$ , respectively. From Figure 3a,  $\|W(t)\|_F$  of the OZNN model (9), IEZNN model (12) and ADIZNN model (19) can achieve convergence to zero. However, in the comparison of convergence time, the OZNN model (9) is the slowest, and the IEZNN (12) and ADIZNN model (19) can converge within 1.3 and 4.7 s, respectively. Under linear noise, the information suggested by the Figure 3b–d is that the error norms  $\|W(t)\|_F$  of the OZNN model (9) and IEZNN model (12) present a divergence trend. However,  $\|W(t)\|_F$  of the ADIZNN model (19) can converge under the linear noise, and the convergence accuracy can reach  $1 \times 10^{-3}$ . It can be seen that the convergence accuracy of the ADIZNN model (19) does not decrease with the increase of linear noise  $z_i(t)$ . Besides, the detailed comparison of the three models under the four different noises is given in Table 1.

Furthermore, the different parameters of ADIZNN (19) are reported for the DSE with (35) under the noise  $z_i(t) = 16t + 4$  in Figure 4. The parameter  $\lambda = 1$  of the ADIZNN is fixed, and  $\zeta = 1.2$ ,  $\zeta = 2.4$ ,  $\zeta = 3.6$  are selected respectively in Figure 4a. Then, the parameter  $\zeta = 1$  of the ADIZNN is fixed, and  $\lambda = 0.8$ ,  $\lambda = 1.6$ ,  $\lambda = 2.4$  are investigated respectively in Figure 4b. From Figure 4a,b, as  $\zeta$  and  $\lambda$  increase, the convergence speed of ADIZNN (19) becomes faster. By contrast, the gain of parameter  $\lambda$  on the convergence rate of the model is greater than that of parameter  $\zeta$ .

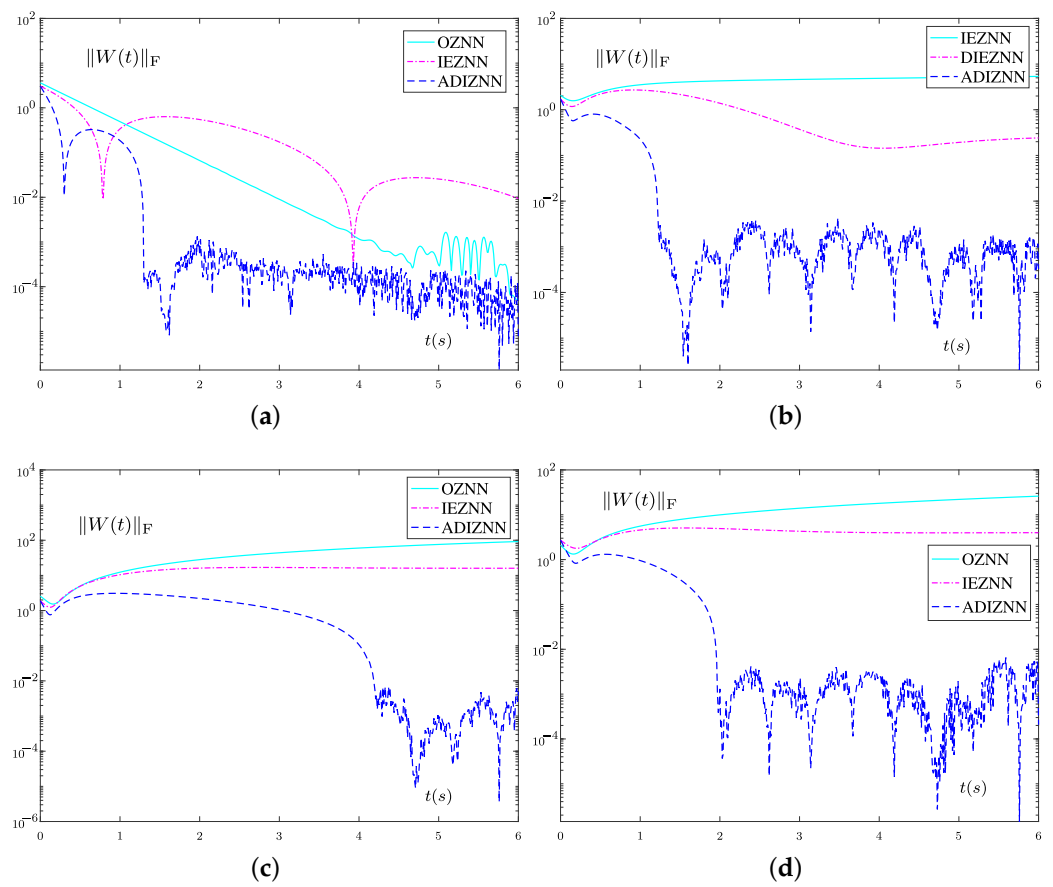


**Figure 3.** Error norms  $\|W(t)\|_F$  of OZNN (9), IEZNN (12) and ADIZNN (19) for the DSE with (35) in different noise environments. (a) No noise  $z_i(t) = 0$ . (b) Linear noise  $z_i(t) = t/4 + 4$ . (c) Linear noise  $z_i(t) = 4t + 4$ . (d) Linear noise  $z_i(t) = 16t + 4$ .

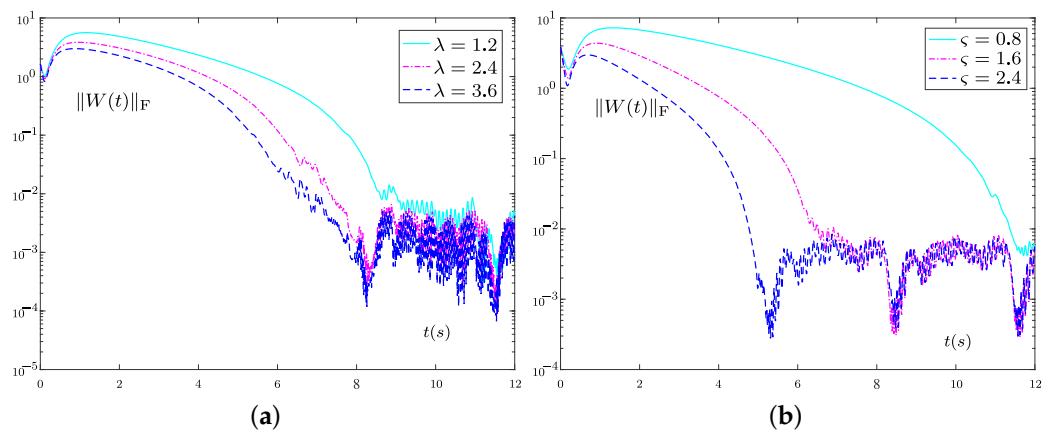


**Figure 4.** Error norms  $\|W(t)\|_F$  of ADIZNN (19) with different parameters for the DSE with (35) in linear noise  $z_i(t) = 16t + 4$ . (a) Fixed  $\lambda = 1$ , different  $\zeta$ . (b) Fixed  $\zeta = 1$ , different  $\lambda$ .

**Table 1.** The detailed comparison of OZNN (9), IEZNN (12) and ADIZNN (19) with  $\zeta = 2$  and  $\lambda = 1$  for the DSE with (35) under the different noise environments.

Noise	OZNN Model (9)	IEZNN Model (12)	ADIZNN Model (19)
$z_i(t) = 0$	convergent	convergent	convergent
$z_i(t) = t/4 + 4$	diverging	diverging	convergent
$z_i(t) = 4t + 4$	diverging	diverging	convergent
$z_i(t) = 16t + 4$	diverging	diverging	convergent

4.2. Experiment 2

Furthermore, the two-dimensional matrices are extended to the four-dimensional matrices are considered:

$$\begin{aligned}
 U(t) &= \begin{bmatrix} s(t) & -s(t) & -s(t) & c(t) \\ s(t) & c(t) & c(t) & s(t) \\ s(t) & -c(t) & c(t) & -s(t) \\ -c(t) & -s(t) & s(t) & c(t) \end{bmatrix}, \\
 V(t) &= \begin{bmatrix} t & 0 & 0 & 0 \\ 0 & \frac{1}{t+1} & 0 & 0 \\ 0 & 0 & t+2 & 0 \\ 0 & 0 & 0 & 1 \end{bmatrix}, G(t) = \begin{bmatrix} s(3t) & s(3t) & s(3t) & c(3t) \\ 0 & s(3t) & c(3t) & c(3t) \\ 0 & 0 & c(3t) & c(3t) \\ 0 & 0 & 0 & c(3t) \end{bmatrix}.
 \end{aligned} \tag{36}$$

The parameters of FTAF (14) are  $\varepsilon_1 = \varepsilon_2 = \varepsilon_3 = \varepsilon_4 = 0.5$  and  $\mu = 0.5, \sigma = 2$ .

Figure 5 presents the error norms  $\|W(t)\|_F$  of OZNN (9), IEZNN (12) and ADIZNN (19) with  $\zeta = 2$  and  $\lambda = 1$  under the different noise environments for the four-dimensional matrices (36). In Figure 5a, all three models can achieve convergence in a noiseless environment, but the convergence rate of ADIZNN (19) is much faster than OZNN (9) and IEZNN (12). However, the convergence time of these three models is very different. ADIZNN (19) can achieve convergence within 1.1 s, OZNN (9) can achieve convergence within 5.2 s, and IEZNN (12) takes a longer time to achieve convergence. Figure 5b–d presents the error norms  $\|W(t)\|_F$  of ADIZNN (19) can achieve convergence, while the error norms of the other two models are diverging. It can be seen that when the noise are  $z_i(t) = t/4 + 4$ ,  $z_i(t) = 4t + 4$  and  $z_i(t) = 16t + 4$ , the convergence time of ADIZNN (19) are 1.1 s, 2.1 s and 4.3 s, respectively. It shows that only ADIZNN (19) can still solve the DSE problem under linear noise well for the high-dimensional matrices.

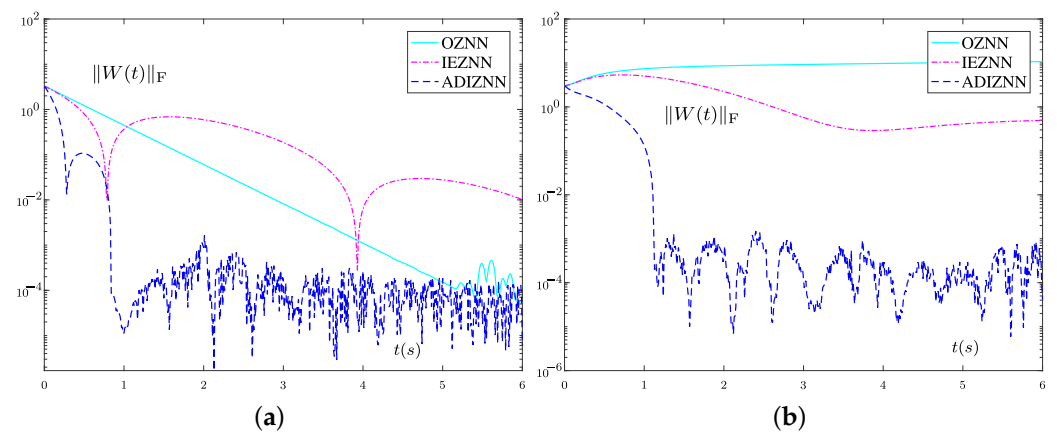
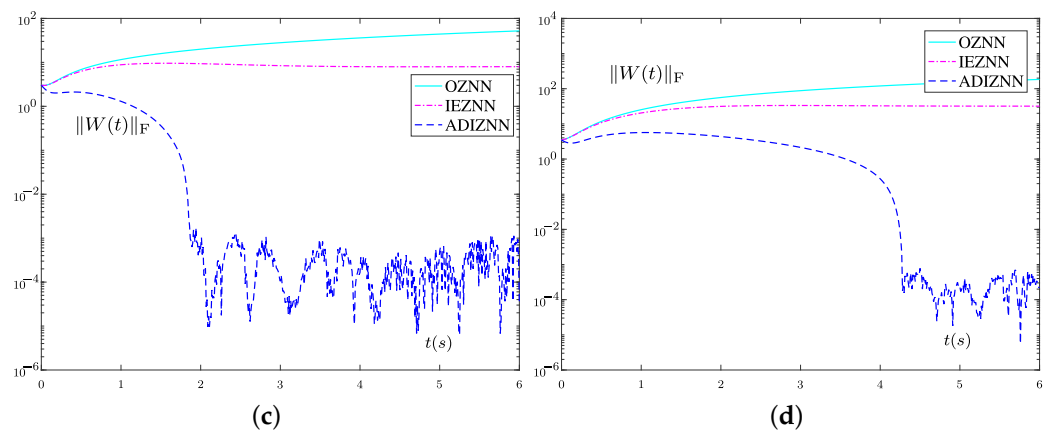


Figure 5. Cont.



**Figure 5.** Error norms  $\|W(t)\|_F$  of OZNN (9), IEZNN (12) and ADIZNN (19) for the DSE with (36) in different noise environments. (a)  $z_i(t) = 0$ . (b)  $z_i(t) = t/4 + 4$ . (c)  $z_i(t) = 4t + 4$ . (d)  $z_i(t) = 16t + 4$ .

**5. Application to the Control of the Sine Function Memristor Chaotic System**

The design method of ZNN can not only be effectively used to solve the DSE, but also can be utilized for the control of the chaotic system. Chaotic system [46] is a kind of common nonlinear systems, which is widely used in secure communication [47,48], power systems and network systems [49–51]. Hence, the SFM chaotic control system [52] and three controllers based on ZNNs are presented in this section.

The SFM [52] is introduced in detail as follows:

$$\begin{cases} \dot{x}_1(t) = s(x_2(t)), \\ \dot{x}_2(t) = -\frac{1}{3}s(x_1(t)) + \frac{1}{2}s(x_2(t)) - \frac{1}{2}\eta^2s(x_2(t))s^2(x_3(t)), \\ \dot{x}_3(t) = -s(x_2(t)) - 0.6s(x_3(t)) + \eta s(x_2(t))s(x_3(t)), \end{cases} \tag{37}$$

where  $X(t) = [x_1(t), x_2(t), x_3(t)]^T$  are state variables.

When considering uncertainties, noise and the controller, (37) is rewritten as

$$\begin{cases} \dot{x}_1(t) = s(x_2(t)) + \Delta f_1(x) + \hbar_1(t) + u_1(t), \\ \dot{x}_2(t) = -\frac{1}{3}s(x_1(t)) + \frac{1}{2}s(x_2(t)) - \frac{1}{2}\eta^2s(x_2(t))s^2(x_3(t)) + \Delta f_2(x) + \hbar_2(t) + u_2(t), \\ \dot{x}_3(t) = -s(x_2(t)) - 0.6s(x_3(t)) + \eta s(x_2(t))s(x_3(t)) + \Delta f_3(x) + \hbar_3(t) + u_3(t), \end{cases} \tag{38}$$

where  $\Delta f_1(x)$ ,  $\Delta f_2(x)$  and  $\Delta f_3(x)$  are uncertainties of the system,  $\hbar_1(t)$ ,  $\hbar_2(t)$  and  $\hbar_3(t)$  refer to external disturbances,  $u_1(t)$ ,  $u_2(t)$  and  $u_3(t)$  represent the controllers.

Define error  $\mathcal{E}(t) = X(t) - 0$ , where  $\mathcal{E}(t) = [e_1(t), e_2(t), e_3(t)]^T$ .

According to design Formula (7), we have

$$\dot{\mathcal{E}}(t) = -\zeta\mathcal{E}(t). \tag{39}$$

Thus, combining (38) and (39), the controller based on OZNN (39) is

$$\begin{cases} u_1(t) = -\zeta x_1(t) - s(x_2(t)), \\ u_2(t) = -\zeta x_2(t) + \frac{1}{3}s(x_1(t)) - \frac{1}{2}s(x_2(t)) + \frac{1}{2}\eta^2s(x_2(t))s^2(x_3(t)), \\ u_3(t) = -\zeta x_3(t) + s(x_2(t)) + 0.6s(x_3(t)) - \eta s(x_2(t))s(x_3(t)). \end{cases} \tag{40}$$

Based on the (10), we get

$$\dot{\mathcal{E}}(t) = -\zeta\mathcal{E}(t) - \lambda \int_0^t \mathcal{E}(\tau) d\tau. \tag{41}$$

Similarly, combining (38) and (41), we have the controller based on IEZNN (41) as follows:

$$\begin{cases} u_1(t) = -\zeta x_1(t) - \lambda \int_0^t x_1(\tau) d\tau - s(x_2(t)), \\ u_2(t) = -\zeta x_2(t) - \lambda \int_0^t x_2(\tau) d\tau + \frac{1}{3}s(x_1(t)) - \frac{1}{2}s(x_2(t)) + \frac{1}{2}\eta^2 s(x_2(t))s^2(x_3(t)), \\ u_3(t) = -\zeta x_3(t) - \lambda \int_0^t x_3(\tau) d\tau + s(x_2(t)) + 0.6s(x_3(t)) - \eta s(x_2(t))s(x_3(t)). \end{cases} \tag{42}$$

Analogously, the design formula of the ADIZNN is

$$\begin{aligned} \dot{\mathcal{E}}(t) = & -2\lambda\mathcal{E}(t) - \zeta\Phi(\mathcal{E}(t)) - \lambda^2 \int_0^t \mathcal{E}(\tau) d\tau - 2\lambda\zeta \int_0^t \Phi(\mathcal{E}(\tau)) d\tau \\ & - \lambda^2\zeta \int_0^t \int_0^\tau \Phi(\mathcal{E}(\sigma)) d\sigma d\tau. \end{aligned} \tag{43}$$

Thus, combining (38) and (43), the controller based on ADIZNN (43) is

$$\begin{cases} u_1(t) = -2\lambda x_1(t) - \zeta\phi(x_1(t)) - \lambda^2 \int_0^t x_1(\tau) d\tau - 2\lambda\zeta \int_0^t \phi(x_1(\tau)) d\tau \\ \quad - \lambda^2\zeta \int_0^t \int_0^\tau \phi(x_1(\sigma)) d\sigma d\tau - s(x_2(t)), \\ u_2(t) = -2\lambda x_2(t) - \zeta\phi(x_2(t)) - \lambda^2 \int_0^t x_2(\tau) d\tau - 2\lambda\zeta \int_0^t \phi(x_2(\tau)) d\tau \\ \quad - \lambda^2\zeta \int_0^t \int_0^\tau \phi(x_2(\sigma)) d\sigma d\tau + \frac{1}{3}s(x_1(t)) - \frac{1}{2}s(x_2(t)) + \frac{1}{2}\eta^2 s(x_2(t))s^2(x_3(t)), \\ u_3(t) = -2\lambda x_3(t) - \zeta\phi(x_3(t)) - \lambda^2 \int_0^t x_3(\tau) d\tau - 2\lambda\zeta \int_0^t \phi(x_3(\tau)) d\tau \\ \quad - \lambda^2\zeta \int_0^t \int_0^\tau \phi(x_3(\sigma)) d\sigma d\tau + \frac{1}{3}s(x_1(t)) + \frac{1}{2}s(x_2(t)) - \frac{1}{2}\eta^2 s(x_2(t))s^2(x_3(t)). \end{cases} \tag{44}$$

Let  $\Delta f(x) = [s(x_2(t)), 2c(x_1(t)), 3s(x_1(t))c(x_3(t))]^T$ ,  $\hat{h}(t) = [t/4 + 4] \in \mathbb{R}^{3 \times 1}$  and set the  $\eta = 3$ ,  $\zeta = 2$  and  $\lambda = 1$ , the ADIZNN model using the FTAF with  $\varepsilon_1 = \varepsilon_2 = \varepsilon_3 = \varepsilon_4 = 0.5$  and  $\mu = 0.5$ ,  $\sigma = 2$ . Figure 6a presents space tracks of the original system (37) under no controller. Figure 6b–d indicate space tracks of system (38) under controller (40), controller (42) and controller (44) from initial values  $X(0) = [0.1, 0.1, 0.1]^T$ . The end points of system (38) under controller (40), controller (42) and controller (44) are respectively  $[1266, 1266, 1266]^T$ ,  $[0.9748, 0.9918, -0.0518]^T$  and  $[-0.0033, 0.0047, 9.952 \times 10^{-7}]^T$ . Figure 7a presents states of original system (37). It is obvious from the Figure 7b–d that the state (i.e., errors) of system (38) under controller (40) and controller (42) cannot reach zero in a three-dimensional space. At the same time, the state of and controller (44) can stable to zero. From the above data, it can be seen that the phase of the SFM system under controller (44) is fairly close to zero with a tiny error, and we hope that the end point of the phase of controller is the closest to zero, so as to achieve the smallest error as possible. The experimental results substantiate the effectiveness and feasibility of the controller (44). In other words, a double integral design scheme can also effectively suppress the existing linear noise and other additional interference items in the application of sine function memristor chaotic system control.

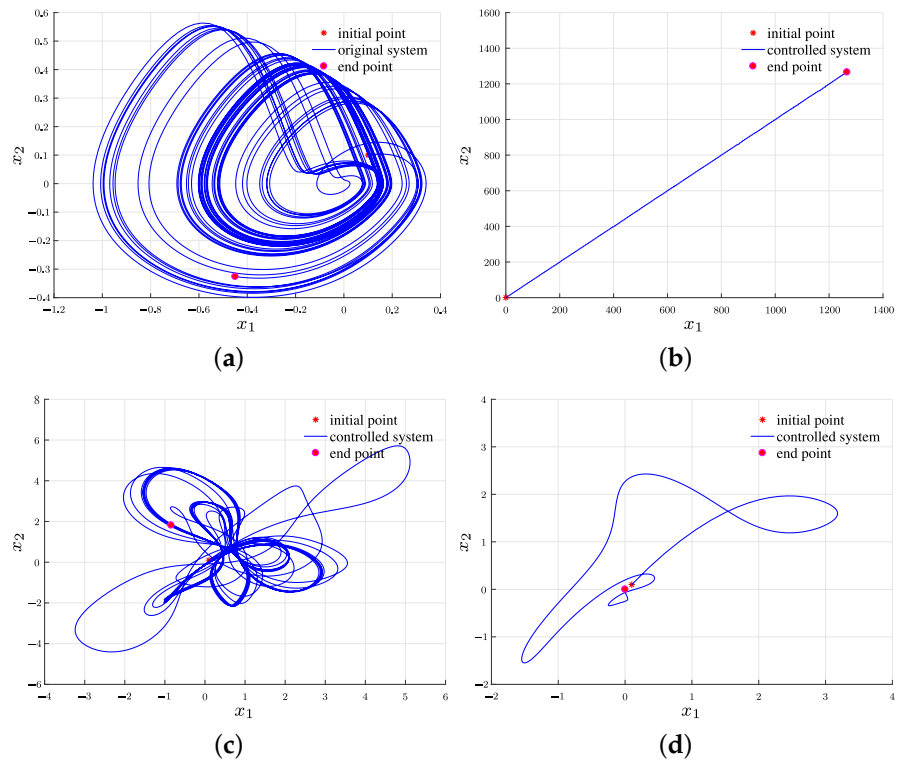


**Figure 6.** Phases of the original SFM system and the SFM under controller (40), controller (42) and controller (44) from  $X(0) = [0.1, 0.1, 0.1]^T$ . (a) Original SFM system; (b) By controller (40); (c) By controller (42); (d) By controller (44).

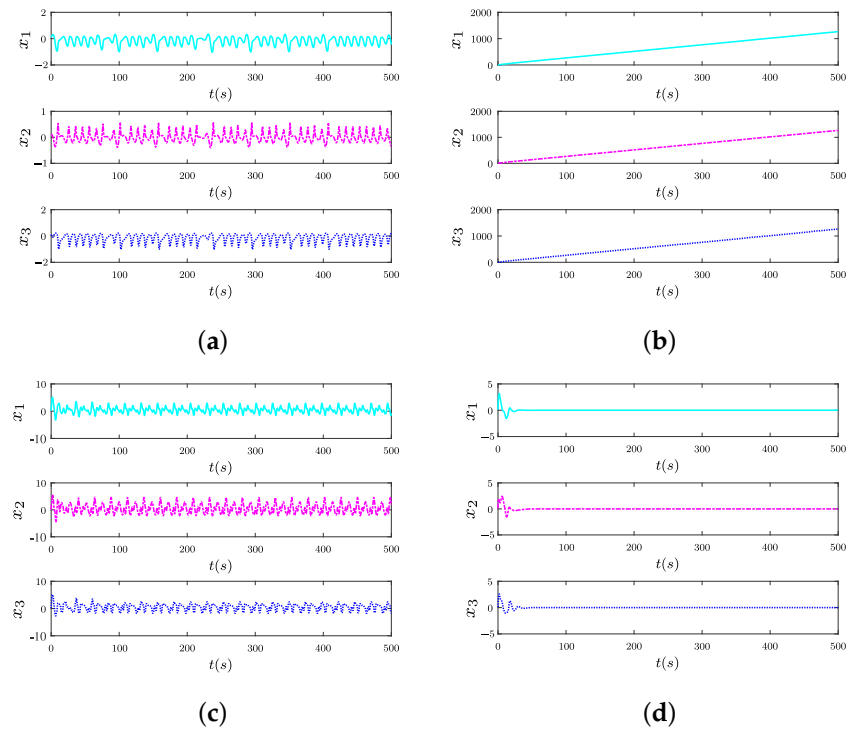


**Figure 7.** State trajectories of the original SFM system and the SFM under controller (40), controller (42) and controller (44) from  $X(0) = [0.1, 0.1, 0.1]^T$ . (a) Original SFM system; (b) By controller (40); (c) By controller (42); (d) By controller (44).

## 6. Conclusions

An innovative ZNN with a double integral was proposed, which can settle the DSE under linear noise. It is worth mentioning that the ADIZNN model has excellent convergence and robustness, which has been verified by theory. Additionally, two different dimensional experiments have revealed that the ADIZNN has more remarkable convergence and anti-noise ability than the OZNN and IEZNN under various linear noises. Finally, phases and states trajectories of the SFM chaotic system synthesized by several controllers have been given to indicate that the controller based on ADIZNN has the highest convergence rate in three-dimensional space.

**Author Contributions:** Conceptualization, L.H. and Y.H.; methodology, C.H. and B.L.; software, Y.H.; validation, L.H. and B.L.; formal analysis, C.H.; investigation, Y.H.; data curation, Y.H. and C.H.; writing—original draft preparation, L.H.; writing—review and editing, B.L. and L.H.; visualization, Y.H.; supervision, B.L. and Y.H.; project administration, B.L.; funding acquisition, B.L. and L.H. All authors have read and agreed to the published version of the manuscript.

**Funding:** This work was funded by the National Natural Science Foundation of China under Grants 62066015 and 61962023; the Natural Science Foundation of Hunan Province of China under grant 2020JJ4511; and the Research Foundation of Education Bureau of Hunan Province of China under Grant 20A396; and the Hunan Provincial Innovation Foundation For Postgraduate under grant CX20221105.

**Institutional Review Board Statement:** Not applicable.

**Informed Consent Statement:** Not applicable.

**Data Availability Statement:** Not applicable.

**Conflicts of Interest:** The authors declare no conflict of interest.

## Abbreviations

The following abbreviations are used in this manuscript:

DSE	Dynamic Sylvester equation
ZNN	Zeroing neural network
OZNN	Original zeroing neural network
ADIZNN	Accelerated double integral ZNN
SFM	Sine function memristor
RNNs	recurrent neural networks
GNN	Gradient neural network
IEZNN	integral enhanced ZNN model
FTAF	fixed-time activation function

## References

- Wei, Q.; Dobigeon, N.; Tourneret, J.Y.; Bioucas-Dias, J.; Godsill, S. R-FUSE: Robust fast fusion of multiband images based on solving a Sylvester equation. *IEEE Signal Process. Lett.* **2016**, *23*, 1632–1636. [[CrossRef](#)]
- Huo, L.; Yang, S.; Jiao, L.; Wang, S.; Shi, J. Local graph regularized coding for salient object detection. *Infrared Phys. Technol.* **2016**, *77*, 124–131. [[CrossRef](#)]
- Shaker, H.R.; Tahavori, M. Control configuration selection for bilinear systems via generalised Hankel interaction index array. *Int. J. Control* **2015**, *88*, 30–37. [[CrossRef](#)]
- Dolgov, S.; Pearson, J.W.; Savostyanov, D.V.; Stoll, M. Fast tensor product solvers for optimization problems with fractional differential equations as constraints. *Appl. Math. Comput.* **2016**, *273*, 604–623. [[CrossRef](#)]
- Jin, L.; Yan, J.; Du, X.; Xiao, X.; Fu, D. RNN for solving time-variant generalized Sylvester equation with applications to robots and acoustic source localization. *IEEE Trans. Ind. Inform.* **2020**, *16*, 6359–6369. [[CrossRef](#)]
- Katsikis, V.N.; Mourtas, S.D.; Stanimirović, P.S.; Zhang, Y. Solving complex-valued time-varying linear matrix equations via QR decomposition with applications to robotic motion tracking and on angle-of-arrival localization. *IEEE Trans. Neural Netw. Learn. Syst.* **2021**, *33*, 3415–3424. [[CrossRef](#)] [[PubMed](#)]
- Li, W.; Han, L.; Xiao, X.; Liao, B.; Peng, C. A gradient-based neural network accelerated for vision-based control of an RCM-constrained surgical endoscope robot. *Neural Comput. Appl.* **2022**, *34*, 1329–1343. [[CrossRef](#)]

8. Li, Z.; Liao, B.; Xu, F.; Guo, D. A new repetitive motion planning scheme with noise suppression capability for redundant robot manipulators. *IEEE Trans. Syst. Man Cybern. Syst.* **2018**, *50*, 5244–5254. [[CrossRef](#)]
9. Liao, B.; Han, L.; Cao, X.; Li, S.; Li, J. Double integral-enhanced Zeroing neural network with linear noise rejection for time-varying matrix inverse. *CAAI Trans. Intell. Technol.* **2023**, 1–14. [[CrossRef](#)]
10. Yan, X.; Liu, M.; Jin, L.; Li, S.; Hu, B.; Zhang, X.; Huang, Z. New zeroing neural network models for solving nonstationary Sylvester equation with verifications on mobile manipulators. *IEEE Trans. Ind. Inform.* **2019**, *15*, 5011–5022. [[CrossRef](#)]
11. Song, C.; Feng, J.; Wang, X.; Zhao, J. Finite iterative method for solving coupled Sylvester-transpose matrix equations. *J. Appl. Math. Comput.* **2014**, *46*, 351–372. [[CrossRef](#)]
12. Ali Beik, F.P.; Movahed, F.S.; Ahmadi-Asl, S. On the Krylov subspace methods based on tensor format for positive definite Sylvester tensor equations. *Numer. Linear Algebra Appl.* **2016**, *23*, 444–466. [[CrossRef](#)]
13. Wu, H.C.; Chen, T.C.T.; Chiu, M.C. Constructing a precise fuzzy feedforward neural network using an independent fuzzification approach. *Axioms* **2021**, *10*, 282. [[CrossRef](#)]
14. Tuyen, D.N.; Tuan, T.M.; Le, X.H.; Tung, N.T.; Chau, T.K.; Van Hai, P.; Gerogiannis, V.C.; Son, L.H. RainPredRNN: A new approach for precipitation nowcasting with weather radar echo images based on deep learning. *Axioms* **2022**, *11*, 107. [[CrossRef](#)]
15. Su, L.; Zhou, L. Exponential synchronization of memristor-based recurrent neural networks with multi-proportional delays. *Neural Comput. Appl.* **2019**, *31*, 7907–7920. [[CrossRef](#)]
16. Khan, A.H.; Li, S.; Luo, X. Obstacle avoidance and tracking control of redundant robotic manipulator: An RNN-based metaheuristic approach. *IEEE Trans. Ind. Inform.* **2019**, *16*, 4670–4680. [[CrossRef](#)]
17. Jin, L.; Li, S.; Hu, B. RNN models for dynamic matrix inversion: A control-theoretical perspective. *IEEE Trans. Ind. Inform.* **2017**, *14*, 189–199. [[CrossRef](#)]
18. He, X.; Liu, Q.; Yang, Y. MV-GNN: Multi-view graph neural network for compression artifacts reduction. *IEEE Trans. Image Process.* **2020**, *29*, 6829–6840. [[CrossRef](#)]
19. Zhang, Y.; Jiang, D.; Wang, J. A recurrent neural network for solving Sylvester equation with time-varying coefficients. *IEEE Trans. Neural Netw.* **2002**, *13*, 1053–1063. [[CrossRef](#)]
20. Zhang, Z.; Zheng, L.; Weng, J.; Mao, Y.; Lu, W.; Xiao, L. A new varying-parameter recurrent neural-network for online solution of time-varying Sylvester equation. *IEEE Trans. Cybern.* **2018**, *48*, 3135–3148. [[CrossRef](#)] [[PubMed](#)]
21. Xiao, L.; Zhang, Z.; Zhang, Z.; Li, W.; Li, S. Design, verification and robotic application of a novel recurrent neural network for computing dynamic Sylvester equation. *Neural Netw.* **2018**, *105*, 185–196. [[CrossRef](#)]
22. Qiu, B.; Zhang, Y.; Yang, Z. New discrete-time ZNN models for least-squares solution of dynamic linear equation system with time-varying rank-deficient coefficient. *IEEE Trans. Neural Netw. Learn. Syst.* **2018**, *29*, 5767–5776. [[CrossRef](#)] [[PubMed](#)]
23. He, Y.; Liao, B.; Xiao, L.; Han, L.; Xiao, X. Double accelerated convergence ZNN with noise-suppression for handling dynamic matrix inversion. *Mathematics* **2021**, *10*, 50. [[CrossRef](#)]
24. Xiao, L.; He, Y.; Li, Y.; Dai, J. Design and analysis of two nonlinear ZNN models for matrix LR and QR factorization with application to 3D moving target location. *IEEE Trans. Ind. Inform.* **2022**, 1–11. [[CrossRef](#)]
25. Katsikis, V.N.; Mourtas, S.D.; Stanimirović, P.S.; Zhang, Y. Continuous-time varying complex QR decomposition via zeroing neural dynamics. *Neural Process Lett.* **2021**, *53*, 3573–3590. [[CrossRef](#)]
26. Xiao, L.; He, Y. A noise-suppression ZNN model with new variable parameter for dynamic Sylvester equation. *IEEE Trans. Ind. Inform.* **2021**, *17*, 7513–7522. [[CrossRef](#)]
27. Tang, G.; Li, X.; Xu, Z.; Li, S.; Zhou, X. An integration-enhanced noise-resistant RNN model with superior performance illustrated via time-varying Sylvester equation solving. In Proceedings of the IEEE 2020 Chinese Control And Decision Conference (CCDC), Hefei, China, 22–24 August 2020; pp. 1906–1911.
28. Gong, J.; Jin, J. A faster and better robustness zeroing neural network for solving dynamic Sylvester equation. *Neural Process Lett.* **2021**, *53*, 3591–3606. [[CrossRef](#)]
29. Han, L.; Liao, B.; He, Y.; Xiao, X. Dual noise-suppressed ZNN with predefined-time convergence and its application in matrix inversion. In Proceedings of the IEEE 2021 11th International Conference on Intelligent Control and Information Processing (ICICIP), Denver, CO, USA, 28–30 September 2021; pp. 410–415.
30. Xiao, L.; He, Y.; Dai, J.; Liu, X.; Liao, B.; Tan, H. A variable-parameter noise-tolerant zeroing neural network for time-variant matrix inversion with guaranteed robustness. *IEEE Trans. Neural Netw. Learn. Syst.* **2020**, *33*, 1535–1545. [[CrossRef](#)]
31. Guo, D.; Li, S.; Stanimirović, P.S. Analysis and application of modified ZNN design with robustness against harmonic noise. *IEEE Trans. Ind. Inform.* **2019**, *16*, 4627–4638. [[CrossRef](#)]
32. Jin, L.; Zhang, Y.; Li, S. Integration-enhanced Zhang neural network for real-time-varying matrix inversion in the presence of various kinds of noises. *IEEE Trans. Neural Netw. Learn. Syst.* **2015**, *27*, 2615–2627. [[CrossRef](#)]
33. Dzieciol, H.; Sillekens, E.; Lavery, D. Extending phase noise tolerance in UDWDM access networks. In Proceedings of the 2020 IEEE Photonics Society Summer Topicals Meeting Series (SUM), Virtual, 13–15 July 2020; pp. 1–2.
34. Xiang, Q.; Liao, B.; Xiao, L.; Jin, L. A noise-tolerant Z-type neural network for time-dependent pseudoinverse matrices. *Optik* **2018**, *165*, 16–28. [[CrossRef](#)]
35. Johnson, M.A.; Moradi, M.H. *PID Control*; Springer: Berlin/Heidelberg, Germany, 2005.
36. Liao, B.; Han, L.; He, Y.; Cao, X.; Li, J. Prescribed-time convergent adaptive ZNN for time-varying matrix inversion under harmonic noise. *Electronics* **2022**, *11*, 1636. [[CrossRef](#)]

37. Jin, J.; Qiu, L. A robust fast convergence zeroing neural network and its applications to dynamic Sylvester equation solving and robot trajectory tracking. *J. Frankl. Inst.* **2022**, *359*, 3183–3209. [[CrossRef](#)]
38. Zhang, Y.; Yi, C.; Guo, D.; Zheng, J. Comparison on Zhang neural dynamics and gradient-based neural dynamics for online solution of nonlinear time-varying equation. *Neural Comput. Appl.* **2011**, *20*, 1–7. [[CrossRef](#)]
39. Zhang, Y.; Jin, L.; Ke, Z. Superior performance of using hyperbolic sine activation functions in ZNN illustrated via time-varying matrix square roots finding. *Comput. Sci. Inf. Syst.* **2012**, *9*, 1603–1625. [[CrossRef](#)]
40. Yang, Y.; Zhang, Y. Superior robustness of power-sum activation functions in Zhang neural networks for time-varying quadratic programs perturbed with large implementation errors. *Neural Comput. Appl.* **2013**, *22*, 175–185. [[CrossRef](#)]
41. Zhang, Y.; Ding, Y.; Qiu, B.; Zhang, Y.; Li, X. Signum-function array activated ZNN with easier circuit implementation and finite-time convergence for linear systems solving. *Inf. Process. Lett.* **2017**, *124*, 30–34. [[CrossRef](#)]
42. Benner, P. Factorized solution of Sylvester equations with applications in control. *Sign (H)* **2004**, *1*, 2.
43. Castelan, E.B.; da Silva, V.G. On the solution of a Sylvester equation appearing in descriptor systems control theory. *Syst. Control Lett.* **2005**, *54*, 109–117. [[CrossRef](#)]
44. Wei, Q.; Dobigeon, N.; Tournet, J.Y. Fast fusion of multi-band images based on solving a Sylvester equation. *IEEE Trans. Image Process.* **2015**, *24*, 4109–4121. [[CrossRef](#)]
45. Diao, H.; Shi, X.; Wei, Y. Effective condition numbers and small sample statistical condition estimation for the generalized Sylvester equation. *Sci. China Math.* **2013**, *56*, 967–982. [[CrossRef](#)]
46. Zhang, R.; Xi, X.; Tian, H.; Wang, Z. Dynamical analysis and finite-time synchronization for a chaotic system with hidden attractor and surface equilibrium. *Axioms* **2022**, *11*, 579. [[CrossRef](#)]
47. Rasouli, M.; Zare, A.; Hallaji, M.; Alizadehsani, R. The synchronization of a class of time-delayed chaotic systems using sliding mode control based on a fractional-order nonlinear PID sliding surface and its application in secure communication. *Axioms* **2022**, *11*, 738. [[CrossRef](#)]
48. He, W.; Luo, T.; Tang, Y.; Du, W.; Tian, Y.C.; Qian, F. Secure communication based on quantized synchronization of chaotic neural networks under an event-triggered strategy. *IEEE Trans. Neural Netw. Learn. Syst.* **2019**, *31*, 3334–3345. [[CrossRef](#)] [[PubMed](#)]
49. Xiao, L.; He, Y.; Liao, B. A parameter-changing zeroing neural network for solving linear equations with superior fixed-time convergence. *Expert Syst. Appl.* **2022**, *208*, 118086. [[CrossRef](#)]
50. Su, H.; Luo, R.; Huang, M.; Fu, J. Robust fixed time control of a class of chaotic systems with bounded uncertainties and disturbances. *Int. J. Control Autom. Syst.* **2022**, *20*, 813–822. [[CrossRef](#)]
51. Singer, J.; Wang, Y.; Bau, H.H. Controlling a chaotic system. *Phys. Rev. Lett.* **1991**, *66*, 1123. [[CrossRef](#)]
52. Sun, J.; Zhao, X.; Fang, J.; Wang, Y. Autonomous memristor chaotic systems of infinite chaotic attractors and circuitry realization. *Nonlinear Dyn.* **2018**, *94*, 2879–2887. [[CrossRef](#)]

**Disclaimer/Publisher’s Note:** The statements, opinions and data contained in all publications are solely those of the individual author(s) and contributor(s) and not of MDPI and/or the editor(s). MDPI and/or the editor(s) disclaim responsibility for any injury to people or property resulting from any ideas, methods, instructions or products referred to in the content.